

# Self-similar implosions and explosions of radiatively cooling gaseous masses

Mikhail Basko<sup>a)</sup> and Masakatsu Murakami

*Institute of Laser Engineering, Osaka University, Suita, Osaka 565, Japan*

(Received 1 May 1997; accepted 12 November 1997)

A self-similar solution of the gas dynamics equations with heat conduction, which describes homologous contraction and expansion of gaseous masses with a free external boundary, is investigated in detail. As a primary application, implosion of deuterium–tritium (DT) fuel in inertial confinement fusion targets is considered. For strongly non-adiabatic implosions the self-similar solution predicts that the flow pattern should approach an asymptotical regime in which it ceases to depend on the initial entropy. For DT masses relevant to inertial confinement fusion (ICF) this regime begins to dominate at  $\alpha U_{im} \geq 6 \times 10^8$  cm/s, where  $\alpha = p/p_{deg}$  is the fuel isentrope parameter, and  $U_{im}$  is its implosion velocity. The solution has also a branch which describes an asymptotical regime of explosive expansion after an ultra-fast initial heating to a strongly radiating state.

© 1998 American Institute of Physics. [S1070-664X(98)02202-2]

## I. INTRODUCTION

Self-similar solutions play an important role in many branches of physics, and especially in the physics of hydrodynamic phenomena.<sup>1,2</sup> In many situations of practical interest, they greatly facilitate qualitative and parametric analysis of complex hydrodynamic flows and provide useful scaling relationships. Also, they often represent asymptotical flow regimes approached by a whole family of hydrodynamic solutions after the information about certain aspects of the initial state is “forgotten.”

Among a large variety of self-similar solutions of the hydrodynamic equations, those which include heat conduction are relatively few.<sup>3</sup> For this reason alone they attract special attention, and especially so if they find an application to practical problems. A good example is the Pakula–Sigel solution<sup>4</sup> for a planar ablation wave driven by radiative heat conduction, which is widely applied to analyze X-ray hohlraums in the indirect drive approach to inertial confinement fusion (ICF).<sup>5–8</sup> One more example is provided by the self-similar solutions obtained in Refs. 9–11, which allow one to investigate the effect of heat conduction on the propagation of blast waves in an ambient gas with power-law initial density profiles. Of particular interest to ICF is the solution of Refs. 10, 11, which—due to the unique properties of the  $r^{-1}$  density profile—can incorporate in addition to heat conduction also the kinetics of thermonuclear burn and the energy transport by fast  $\alpha$ -particles.

In this paper we present another type of self-similar solution with heat conduction relevant to ICF. As contrasted to those of Refs. 9–11, our solution describes hydrodynamic contraction (or expansion) of a finite gaseous mass with a free boundary which suffers energy losses by radiative heat conduction. Despite its mathematical simplicity, this solution

has eluded proper attention in the literature and appears to have been introduced for the first time in the recent publications by one of the authors.<sup>12,13</sup> Here we expand the results of Ref. 13 and carry out a comprehensive mathematical analysis of this solution, and clarify the physical meaning and interpretation of its key parameters and different branches. We demonstrate that this solution can be applied to the investigation of the effect of radiative cooling on the implosion dynamics of deuterium–tritium (DT) masses with a quasi-uniform (as in the volume ignition and fast ignitor schemes of ICF) entropy distribution, as well as to describe radiative explosions of very rapidly heated (as, for example, with femtosecond laser pulses) particles of matter.

The structure of the paper is as follows. In Sec. II the separation ansatz and similarity variables are introduced for the basic fluid equations. Spatial profiles of the main thermodynamic variables and hydrodynamic stability are discussed in Sec. III. Section IV is devoted to the analysis of the implosion solutions, with the application to implosion of the DT fuel in ICF targets. Section V contains results for solutions which describe an asymptotical regime of radiative explosion after instantaneous heating to a very high temperature. In Sec. VI the main results are summarized.

## II. SEPARATION ANSATZ FOR THE HYDRODYNAMIC EQUATIONS

We start with the one-dimensional hydrodynamic equations,

$$\frac{\partial \rho}{\partial t} + \frac{1}{r^s} \frac{\partial}{\partial r} (\rho u r^s) = 0, \quad (1)$$

$$\frac{\partial u}{\partial t} + u \frac{\partial u}{\partial r} + \frac{1}{\rho} \frac{\partial p}{\partial r} = 0, \quad (2)$$

$$\frac{\partial \epsilon}{\partial t} + u \frac{\partial \epsilon}{\partial r} + \frac{p}{\rho} \frac{1}{r^s} \frac{\partial}{\partial r} (u r^s) = \frac{1}{\rho r^s} \frac{\partial}{\partial r} \left( r^s \kappa \frac{\partial T}{\partial r} \right), \quad (3)$$

<sup>a)</sup>On leave from the Institute for Theoretical and Experimental Physics, B. Chermushkinskaya 25, Moscow 117259, Russia. Electronic mail: basko@vittep5.itrep.ru

which include the heat conduction term on the right-hand side (rhs) of the energy equation (3). Here  $s=0, 1,$  and  $2$  correspond, respectively, to the planar, cylindrical, and spherical flow patterns. We assume the ideal gas equation of state and choose the unit of temperature  $T$  such that

$$p = \rho T, \quad \epsilon = \frac{T}{\gamma - 1}, \tag{4}$$

where  $p$  is the pressure,  $\epsilon$  is the specific internal energy per unit mass, and  $\gamma$  is the adiabatic index. For the heat conduction coefficient  $\kappa$  we assume a power law dependence,

$$\kappa = \kappa_* \rho^{-m} T^n, \tag{5}$$

on the density  $\rho$  and temperature  $T$ , with  $\kappa_*, m,$  and  $n$  being constants. With an intention to apply our solution primarily to the case of radiative heat conduction, we can express  $\kappa$  as

$$\kappa = \frac{16}{3} \sigma_{SB} l_R T^3, \tag{6}$$

where

$$l_R = l_* \rho^{-m} T^{n-3} \tag{7}$$

is the Rosseland mean free path,  $\sigma_{SB}$  is the Stefan-Boltzmann constant, and  $l_* = \frac{3}{16} \kappa_* / \sigma_{SB}$  is a constant.

We are looking for a solution of Eqs. (1)–(3) in the form

$$u = \xi \dot{R}(t), \quad \xi \stackrel{\text{def}}{=} \frac{r}{R(t)}, \tag{8}$$

$$p = p_c(t) \Pi(\xi), \tag{9}$$

$$T = T_c(t) Z(\xi), \tag{10}$$

which belongs to a wide class of self-similar flows with velocity  $u$  being proportional to radius  $r^1$ . A dot over  $R$  indicates the time derivative. The self-similar variable  $\xi$  is a Lagrangian coordinate associated with the mass of the fluid: for any fixed value of  $\xi$  the fluid mass within the interval  $0 \leq r \leq \xi R(t)$  is conserved. We assume that the eigenfunctions  $\Pi(\xi)$  and  $Z(\xi)$  are normalized to  $\Pi(0) = 1, Z(0) = 1$ , so that  $p_c(t)$  and  $T_c(t)$  are, respectively, the central pressure and temperature at  $r = 0$ .

By virtue of the ansatz (8)–(10), the original equations (1)–(3) are reduced to

$$\rho_c R^{s+1} = M_*, \tag{11}$$

$$\frac{R \ddot{R}}{T_c} = - \frac{Z}{\xi \Pi} \frac{d\Pi}{d\xi} = 1, \tag{12}$$

$$\begin{aligned} & \left[ \frac{1}{\gamma - 1} \frac{\dot{T}_c}{T_c} + (s + 1) \frac{\dot{R}}{R} \right] \frac{\rho_c^{m+1} R^2}{\kappa_* T_c^n} \\ & = \frac{1}{\xi^s \Pi} \frac{d}{d\xi} \left( \xi^s \frac{Z^{m+n}}{\Pi^m} \frac{dZ}{d\xi} \right) = -\beta, \end{aligned} \tag{13}$$

where  $\rho_c(t) = p_c(t) / T_c(t)$ , and  $M_*$  is a constant. Having the separation constant in Eq. (12) set equal to unity means no loss of generality because this can always be achieved by a proper normalization of  $R$  and  $\xi$ . But then the interval  $0 \leq \xi \leq \xi_1$  of  $\xi$  variation is to be determined by solving the

eigenvalue problem. The positive sign of the separation constant in Eq. (12) means that we intend to investigate the motions of gaseous masses under zero external pressure. If, instead, we would choose the minus sign, we would recover the Kidder type solutions for implosions driven by external pressure with a certain temporal profile.<sup>14</sup> With the negative sign for the separation constant in Eq. (13), we are looking for a positive eigenvalue  $\beta > 0$  that would correspond to the net cooling of the considered mass.

### III. SPATIAL PROFILES

#### A. Formulation and solution of the eigenvalue problem

Spatial profiles of pressure,  $\Pi(\xi)$ , and temperature,  $Z(\xi)$ , are obtained by integrating the spatial components of Eqs. (12) and (13),

$$Z \frac{d\Pi}{d\xi} + \xi \Pi = 0, \tag{14a}$$

$$\frac{d}{d\xi} \left( \xi^s \frac{Z^{m+n}}{\Pi^m} \frac{dZ}{d\xi} \right) + \beta \xi^s \Pi = 0, \tag{14b}$$

which comprise a third-order system of ordinary differential equations, and for which there are three obvious boundary conditions:

$$\Pi(0) = 1, \quad Z(0) = 1, \quad \frac{dZ(0)}{d\xi} = 0. \tag{15}$$

To be able to determine a unique value of parameter  $\beta$ , we need a fourth boundary condition, which is less obvious and requires some additional justification.

First of all note that, as can be immediately ascertained by straightforward integration of Eq. (14b), the energy flux at the outer boundary  $\xi = \xi_1$  of our gaseous mass, proportional to  $-Z^{n+m} \Pi^{-m} (dZ/d\xi) |_{\xi=\xi_1}$ , is always positive for  $\beta > 0$ . If this boundary is free, the physical mechanism of practical interest by which the energy could escape the gas is thermal radiation. An appropriate boundary condition for radiative losses from a free boundary in the conduction approximation would be

$$-\kappa \frac{\partial T}{\partial r} = 2 \sigma_{SB} T^4$$

(for more details see Sec. 15, Chap. II in Ref. 2). However, in view of our separation ansatz (11)–(13), the latter would imply that the product  $T_c^{n-3} R^{m(s+1)-1}$  must be constant in time, which cannot be satisfied (at least not for the general choice of  $s, m, n,$  and  $\gamma$  values). Hence, we adopt a simpler version of this boundary condition (which is practically no less accurate in the limit of large optical thickness) by setting the boundary temperature equal to zero. In combination with the definition of the outer boundary as a position where the density vanishes, we end up with two additional conditions:

$$\Pi(\xi_1) = Z(\xi_1) = 0, \tag{16}$$

to determine the values of  $\xi_1$  and  $\beta$ .

TABLE I. Principal parameters of the eigenvalue problem.

$s$	$m$	$n$	$\beta$	$\xi_1$	$\gamma_c$
2	2	4	1.2713998	2.2930	1.735508
2	2	5	1.0915617	2.4813	1.571966
2	2	6.5	0.90050252	2.7415	1.428913
2	1	4	0.91052410	2.8498	1.435767
2	1	5	0.76166482	3.1353	1.340282
2	1	6.5	0.61167599	3.5263	1.256111
1	2	6.5	0.57582596	2.7835	1.404323
0	2	6.5	0.26874812	2.8388	1.367518

Note that in the previous publications<sup>12,13</sup> the separation constant  $\beta$  ( $c_b$  in notation of Refs. 12, 13) was treated as a free parameter. For the case of the thermonuclear spark considered in Ref. 12, this was justified by the presence of an outer cold gas layer. The value of  $\beta$  chosen in Ref. 13 to represent the implosion of a DT sphere with a free boundary is actually very close to the one calculated with the boundary condition (16).

In Appendix A it is shown that the eigenvalue problem (14)–(16) always has a solution with finite and positive values of  $\beta$  and  $\xi_1$ , provided that  $m > 0$  and  $n > 0$ . The asymptotical behavior of  $\Pi(\xi)$  and  $Z(\xi)$  for  $\xi \rightarrow \xi_1$  is given by Eqs. (A4). The values of  $\beta$  and  $\xi_1$  calculated for certain combinations of  $s$ ,  $m$ , and  $n$  are listed in Table I. Figure 1 displays the normalized profiles of the pressure, temperature, density, and specific entropy [as defined by Eq. (17) below] for a spherical mass ( $s = 2$ ) with the inverse bremsstrahlung opacity mechanism ( $m = 2$ ,  $n = 13/2$ ).

A question of interest is the relation of the above eigenvalue problem to the adiabatic limit, when the rhs of the energy equation (3) is identically zero. This is not equivalent to simply putting  $\beta = 0$  because the equation (14b) should be omitted altogether in this case, i.e., we are left with one equation (14a) for the two unknown functions  $\Pi(\xi)$  and  $Z(\xi)$ . The latter reflects a well-known fact (see Sec. 29, Chap. I in Ref. 2) that in the adiabatic case one profile function can be chosen arbitrarily. In the non-adiabatic case, this

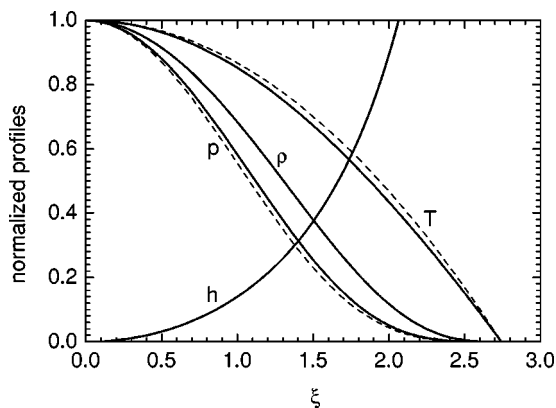


FIG. 1. Normalized spatial profiles of pressure  $p$ , density  $\rho$ , temperature  $T$ , and specific entropy  $h$  as obtained by solving numerically the eigenvalue problem (14)–(16) for the basic set (19) of geometry and material parameters. Dashed curves show the approximate formulae (A6) plotted with the value of  $\xi_1$  taken from Table I.

freedom is eliminated by the additional equation (14b) with the boundary conditions (15) and (16). As a result, we calculate unique profiles of the thermodynamic functions. Clearly, these same profiles can be used in the adiabatic limit [recovered formally from Eq. (13) by putting  $\kappa_* = 0$ ] as well.

**B. Hydrodynamic stability**

With the pressure and density profiles known, we can address the issue of hydrodynamic stability. As it is seen from Eq. (12), the acceleration of all fluid elements is always positive, i.e. directed away from the center. Since the density gradient (see Fig. 1) is everywhere negative, no Rayleigh–Taylor type (heavy fluid on top of light fluid) instability is anticipated. However, a convective instability—similar to what occurs in stellar interiors<sup>15</sup>—is still possible. The Schwarzschild criterion for stability with respect to small adiabatic perturbations<sup>15</sup> requires the specific entropy

$$h = \frac{1}{\gamma - 1} \ln T - \ln \rho = \frac{1}{\gamma - 1} \ln \frac{p}{\rho^\gamma} \tag{17}$$

to increase monotonically upward, i.e., against the gravity or in the direction of acceleration.

In our case the temperature and density profiles are independent of  $\gamma$ , while the entropy gradient depends on  $\gamma$ . As a consequence, our solution is always stable for large enough  $\gamma$ , and may become convectively unstable for  $\gamma$  values close to unity. A closer examination reveals that the Schwarzschild criterion is first violated near the center. Then, by expanding  $\Pi(\xi)$  and  $Z(\xi)$  near  $\xi = 0$ , we find the critical value of the adiabatic index,

$$\gamma_c = \left( 1 - \frac{\beta}{s + 1} \right)^{-1} \tag{18}$$

(listed in Table I together with  $\beta$ ). For  $\gamma > \gamma_c$  our solution is stable. For  $\gamma < \gamma_c$  a convectively unstable core may develop in the center. A more definite answer in this latter case requires that a proper account is taken of the (stabilizing) effect of the heat conduction on the perturbation growth. Table I shows that the case of  $\gamma = 5/3$ , for which the  $h$  profile is plotted in Fig. 1, is stable for the  $s, m, n$  combinations of practical interest.

**IV. IMPLOSION TYPE SOLUTIONS**

**A. Equations governing the temporal evolution**

One of the most obvious applications for our self-similar solution is the final stage of implosion of a spherical DT mass in an ICF target.<sup>13</sup> In the volume ignition mode, when a DT mass with a more or less uniform entropy distribution is compressed to  $\langle \rho r \rangle \geq 1 \text{ g/cm}^2$ , the dominant mechanism of energy loss is by means of thermal radiation.<sup>16–19</sup> The opacity mechanism is that of the inverse bremsstrahlung in a hydrogen plasma—which corresponds to  $m = 2$  and  $n = 13/2$  in Eq. (7)<sup>2</sup>—with a possible contribution from the Compton scattering. Also, for the volume ignition mode to be practical, the Rosseland optical thickness of the DT mass must exceed unity,<sup>16,18,19</sup> which justifies the approximation

TABLE II. Structural integrals for spatial profiles.

$s$	$m$	$n$	$I_M$	$I_{\Pi}$	$I_{\rho}$	$I_{\tau}$
2	2	4	1.094557	0.680837	1.319248	1.203859
2	2	5	1.113424	0.731439	1.309899	1.345360
2	2	6.5	1.134499	0.792660	1.299958	1.562321
2	1	4	1.135744	0.797608	1.299793	1.552528
2	1	5	1.152661	0.850547	1.292201	1.805573
2	1	6.5	1.170509	0.910353	1.284547	2.214068
1	2	6.5	0.999965	0.782785	1.298025	1.504128
0	2	6.5	1.295175	1.145140	1.295175	1.430228

of radiative heat conduction assumed in Eq. (3). All these considerations are equally applicable to the final stage of implosion in the fast ignitor scheme of ignition,<sup>20</sup> where only the final temperature of the DT fuel would be lower than in the case of volume ignition. Orienting ourselves to the situation described above, we adopt the set of parameters

$$s=2, \quad m=2, \quad n=\frac{13}{2}, \quad \gamma=\frac{5}{3}, \tag{19}$$

as a central case for numerical estimates and practical formulae given below.

In accord with the logic of self-similar approach, we neglect the complexities of the initial phase of implosion in realistic ICF schemes and adopt an idealized formulation of the problem: the initial conditions are defined in the limit of  $t \rightarrow -\infty$ , when  $R(t) \rightarrow \infty$  and  $\dot{R}(t) < 0$  [time  $t=0$  is the moment of stagnation when  $\dot{R}(0)=0$ ]. Then, the initial state of the imploding gas is fully specified by the values of its mass,

$$M = (4\pi)_s I_M M_* , \tag{20}$$

initial energy,

$$E_- = \lim_{t \rightarrow -\infty} E(t) = \frac{1}{2} (4\pi)_s (s+1) I_{\Pi} M_* U_-^2, \tag{21}$$

and entropy parameter,

$$\Sigma_- = \lim_{t \rightarrow -\infty} \Sigma(t), \quad \Sigma(t) \stackrel{\text{def}}{=} \frac{p_c(t)}{\rho_c^\gamma(t)}. \tag{22}$$

Here

$$U_- = - \lim_{t \rightarrow -\infty} \dot{R}(t), \tag{23}$$

$I_M$  and  $I_{\Pi}$  are dimensionless integrals,

$$I_M = \int_0^{\xi_1} \frac{\Pi}{Z} \xi^s d\xi, \quad I_{\Pi} = \int_0^{\xi_1} \Pi \xi^s d\xi, \tag{24}$$

calculated in the process of integrating Eqs. (14) and listed in Table II, and

$$(4\pi)_s = \begin{cases} 1, & s=0, \\ 2\pi, & s=1, \\ 4\pi, & s=2. \end{cases} \tag{25}$$

To explore the general properties of the non-adiabatic implosions, it is convenient to normalize the main dimensional variables in the temporal components of Eqs. (11)–(13) with respect to the adiabatic limit by introducing

$$v = \frac{\dot{R}(t)}{U_-}, \quad x = \left( \frac{R_{a0}}{R(t)} \right)^{(\gamma-1)(s+1)}, \quad \sigma = \frac{\Sigma(t)}{\Sigma_-}. \tag{26}$$

Here  $R_{a0}$  is the value of  $R(t)$  at maximum compression ( $t=0$ ) of the adiabatic ( $\kappa_* = 0$ ) implosion with the same initial parameters  $M$ ,  $U_-$ , and  $\Sigma_-$ . In this way, a ready comparison can be made with the simple adiabatic case. By integrating the temporal components of Eqs. (11)–(13) for  $\kappa_* = 0$ , we find

$$T_{a0} = aU_-^2, \quad a = \frac{1}{2}(\gamma-1)(s+1), \tag{27}$$

$$\rho_{a0} = \left( \frac{aU_-^2}{\Sigma_-} \right)^{1/(\gamma-1)}, \tag{28}$$

$$R_{a0} = \left[ M_* \left( \frac{\Sigma_-}{aU_-^2} \right)^{1/(\gamma-1)} \right]^{1/(s+1)}, \tag{29}$$

where  $T_{a0}$  and  $\rho_{a0}$  are, respectively, the adiabatic values of the central temperature  $T_c$  and density  $\rho_c$  at stagnation. With this normalization, the equations governing the temporal evolution can be written as

$$\frac{dv}{dx} = - \frac{1}{2} \frac{\sigma}{v}, \tag{30a}$$

$$\frac{d\sigma}{dx} = \frac{1}{2} \lambda \frac{\sigma^{n+1}}{v} x^{n-\nu-1}, \tag{30b}$$

where

$$\lambda = \beta \kappa_* (\gamma-1) a^{n-\nu-1} U_-^{2n-2\nu-1} \Sigma_-^\nu M_*^{-1/(s+1)} \tag{31}$$

is a dimensionless constant characterizing the degree of non-adiabacity, and

$$\nu = \frac{1}{\gamma-1} \left( m + \frac{s}{s+1} \right) > 0. \tag{32}$$

Clearly, for  $\lambda \ll 1$  the implosion is quasi-adiabatic, and for  $\lambda \gg 1$  it is strongly non-adiabatic.

The  $x, v$ -plane can be viewed as a phase plane of the dynamic system described by the temporal components of Eqs. (12) and (13). In contrast to  $R$  and  $t$ , both  $x$  and  $v$  vary within finite limits over the entire process of implosion and subsequent expansion from  $t = -\infty$  to  $t = +\infty$ . Equations (30) should be integrated with the boundary conditions  $v(0) = -1$  and  $\sigma(0) = 1$ . As can be inferred from Eq. (30b), the latter is possible only if the integral  $\int_0^{x_0} x^{n-\nu-1} dx$  converges at the lower limit, i.e., when  $n > \nu$ . Below we consider only such combinations of  $s$ ,  $m$ ,  $n$ , and  $\gamma$  which satisfy this restriction.

Finally, because  $v(x)$  and  $\sigma(x)$  are not single-valued functions, it is convenient to choose the dimensionless velocity  $v$  as an independent variable and rewrite the system (30) as

$$\frac{dx}{dv} = -2 \frac{v}{\sigma}, \tag{33a}$$

$$\frac{d\sigma}{dv} = -\lambda \sigma^n x^{n-\nu-1}, \tag{33b}$$

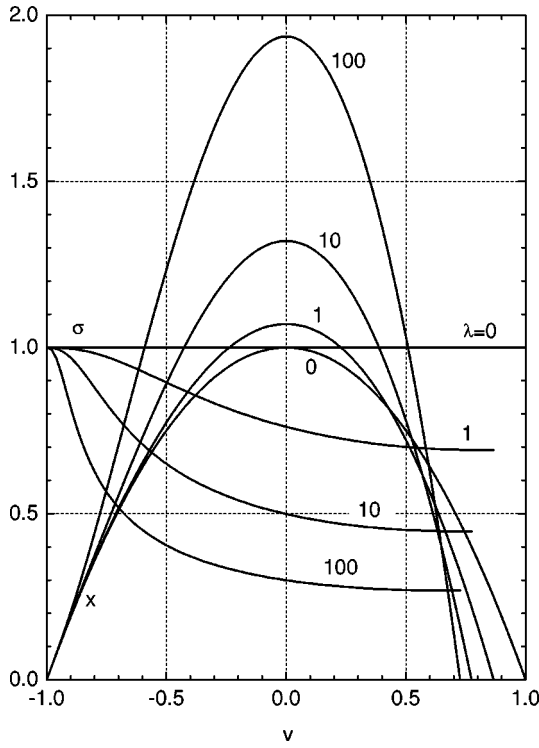


FIG. 2. Integral curves for the system (33) calculated with the basic set (19) of geometry and material parameters for four different values of the non-adiabacity parameter  $\lambda$ . Each curve is marked by the corresponding  $\lambda$  value.

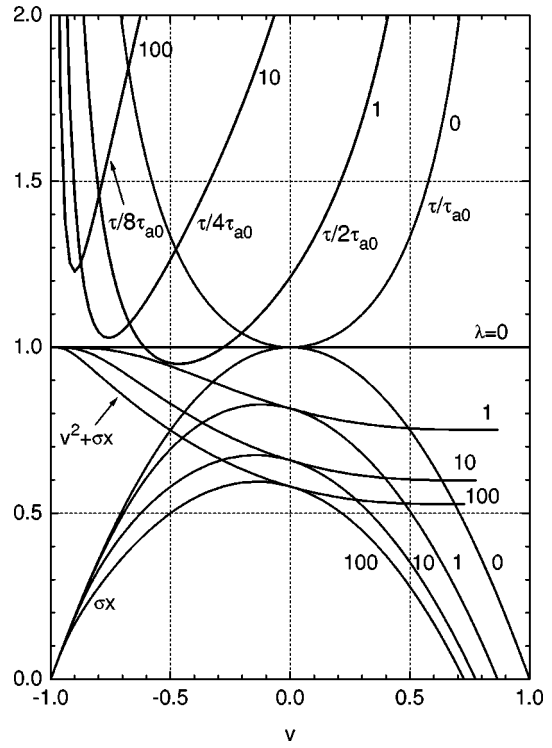


FIG. 3. Normalized temperature,  $\sigma x$ , total energy,  $v^2 + \sigma x$ , and the Roseland optical thickness,  $\tau$ , along the integral curves shown in Fig. 2. Each curve is marked by the corresponding  $\lambda$  value. The  $\tau/\tau_{a0}$  curves for  $\lambda \geq 1$  have been scaled by different factors to have minima around 1.

with the boundary conditions changing to

$$x(-1) = 0, \quad \sigma(-1) = 1. \tag{34}$$

**B. General properties**

The main question we want to address is how do the main characteristics of implosion change with the increasing role of energy loss, i.e., with the increasing value of  $\lambda$ ? The results of numerical integration of Eqs. (33) for the basic set of parameters (19) and for four different values of  $\lambda$  are shown in Figs. 2 and 3. Also, very helpful for gaining insight into qualitative properties of our solution is a particular case of  $n = \nu + 1$ , for which Eqs. (33) can be integrated analytically for any  $\lambda$ . Explicit formulae for this case are given in Appendix B.

The adiabatic limit  $\lambda = 0$  is described by a trivial solution,

$$x = 1 - v^2, \quad \sigma = 1. \tag{35}$$

We remind that  $x = (R_{a0}/R)^2$  in the particular case of  $s = 2$ ,  $\gamma = 5/3$  shown in Figs. 2 and 3, where  $R_{a0}$  is the minimum value of  $R(t)$  for  $\lambda = 0$ . As we increase the value of  $\lambda$ , the stagnation value  $x_0 \equiv x(0)$  of  $x$  increases monotonically to  $\lim_{\lambda \rightarrow \infty} x_0 = \infty$ , while the stagnation value  $\sigma_0 \equiv \sigma(0)$  of  $\sigma$  decreases to  $\lim_{\lambda \rightarrow \infty} \sigma_0 = 0$ . For a particular case of  $n = \nu + 1$  this is readily verified with Eqs. (B1). The general case is analyzed in the next subsection. If we invoke now the expressions for the central density,

$$\rho_c(t) = \rho_{a0} \cdot x^{1/(\gamma-1)}, \tag{36}$$

and the  $\langle \rho r \rangle$  parameter (an important characteristic for the inertial confinement of the thermonuclear fuel),

$$\langle \rho r \rangle(t) = \int_0^{R\xi_1} \rho(t,r) dr = \langle \rho r \rangle_{a0} \cdot x^{s/[(\gamma-1)(s+1)]}, \tag{37}$$

$$\langle \rho r \rangle_{a0} = I_\rho \left[ M_* \left( \frac{aU_-^2}{\Sigma_-} \right)^{s/(\gamma-1)} \right]^{1/(s+1)}, \tag{38}$$

$$I_\rho = \int_0^{\xi_1} \frac{\Pi}{Z} d\xi, \tag{39}$$

we conclude that, within the applicability of our solution, radiative cooling can enhance the density and the  $\langle \rho r \rangle$  of the imploding configuration by an arbitrarily large factor as compared with the adiabatic case. It should be noted that, once the effects of electron degeneracy are taken into account, the density and  $\langle \rho r \rangle$  at stagnation cannot, of course, surpass the values corresponding to the zero isentrope.

The situation is, however, different for the temperature,

$$T_c(t) = T_{a0} \cdot \sigma x, \tag{40}$$

and total energy,

$$E(t) = \frac{1}{2} (4\pi)_s (s+1) I_\Pi M_* U_-^2 \cdot (v^2 + \sigma x), \tag{41}$$

of the imploding mass. As the non-adiabacity parameter  $\lambda$  increases, the product  $\sigma_0 x_0$ , which represents the normalized temperature at stagnation, decreases monotonically but approaches a finite limit,

TABLE III. Parameters which characterize the radiatively dominated regime.

$n$	$\nu$	$\lambda_{rd}$	$\delta_{rd}$	$v_{rd+}$	$\tilde{\sigma}_{rd+}$	$v_{ex+}$	$\sigma_{ex+}$
4	2	11.310346	0.385914	0.574576	0.828839	1.094982	1.096621
4	3	1.254687	0.642857	0.75	0.829827	1.068296	0.978219
4	3.5	0.369853	0.798173	0.848117	0.831594	1.051374	0.863019
6.5	3	110.63482	0.379062	0.585515	0.893985	1.073161	1.116972
6.5	4	12.828483	0.526498	0.691433	0.894067	1.062664	1.083649
6.5	6	0.225866	0.874747	0.906414	0.895187	1.030470	0.921956

$$0 < \delta_{rd} \stackrel{\text{def}}{=} \lim_{\lambda \rightarrow \infty} \sigma_0 x_0 < 1. \tag{42}$$

Again, for  $n = \nu + 1$  this fact can be inferred directly from Eqs. (B1), while the general case is treated in the next subsection. For the basic set (19), the  $\sigma x$  and  $v^2 + \sigma x$  curves are plotted in Fig. 3.

Thus, we arrive at a conclusion that, no matter how strong is the impact of radiative heat conduction on the implosion dynamics, only a fraction  $1 - \delta_{rd}$  (typically on the order of 50%) of the initial energy can be lost by this mechanism. Accordingly, radiative losses can reduce the central temperature at stagnation,  $T_c(0)$ , by only a finite factor  $\delta_{rd}$  as compared to its adiabatic value for the same initial state. Note that this fact has already been recognized in the preceding publication.<sup>13</sup> The exact values of the  $\delta_{rd}$  factor calculated for a selection of  $n$  and  $\nu$  values are given in Table III.

When we compare the  $\sigma$  curves in Fig. 2 with the  $v^2 + \sigma x$  curves in Fig. 3, we see that, whereas most of the initial entropy in the case of  $\lambda \gg 1$  is lost relatively early (well before the stagnation), the main portion of the energy loss occurs just prior to the stagnation, when  $R(t) \leq 2R(0)$ . This is explained by a simple fact that at early times  $t < 0$ , when  $R(t) \gg R(0)$ , the thermal energy is only a small fraction of the total energy. Hence, a significant reduction of the thermal energy at this stage would imply a significant decrease of the entropy but very little change in the total energy.

The  $v > 0$  branch of the integral curves in Figs. 2 and 3 corresponds to the expansion after a bounce at  $v = 0$  ( $t = 0$ ). The effects of non-adiabacity are always relatively mild at this stage for any value of  $\lambda$ . Since part of the initial energy has been lost, the integral curves terminate at a velocity  $0 < v_+ < 1$  defined by the condition

$$x(v_+) = 0, \quad v_+ > 0. \tag{43}$$

As  $\lambda \rightarrow \infty$ , the values of  $v_+$  and of the ratio  $\sigma(v_+)/\sigma_0$  approach finite limits,

$$v_{rd+} \stackrel{\text{def}}{=} \lim_{\lambda \rightarrow \infty} v_+, \quad \tilde{\sigma}_{rd+} \stackrel{\text{def}}{=} \lim_{\lambda \rightarrow \infty} \frac{\sigma(v_+)}{\sigma_0}. \tag{44}$$

The numerical values of these two quantities are also listed in Table III.

### C. Radiatively dominated regime

Because our principal dynamic variables  $x$  and  $\sigma$  become, respectively, infinitely large and infinitely small near stagnation of a strongly non-adiabatic implosion, we must renormalize Eqs. (33) to be able to explore this limit in more detail. Being interested primarily in the parameters at stagnation, we introduce

$$\tilde{x}(v) \stackrel{\text{def}}{=} \frac{x(v)}{x_0}, \quad \tilde{\sigma}(v) \stackrel{\text{def}}{=} \frac{\sigma(v)}{\sigma_0}, \quad \tilde{\phi} = \tilde{\sigma}^{1-n}, \tag{45}$$

and pass to the limit of  $\lambda \rightarrow \infty$  in Eqs. (33) to obtain

$$\frac{d\tilde{x}}{dv} = -\frac{2}{\delta_{rd}} v \tilde{\phi}^{1/(n-1)}, \tag{46a}$$

$$\frac{d\tilde{\phi}}{dv} = (n-1) \lambda_{rd} \delta_{rd}^{n-1} \tilde{x}^{n-\nu-1}, \tag{46b}$$

with the boundary conditions

$$\tilde{x}(-1) = 0, \quad \tilde{\phi}(-1) = 0, \quad \tilde{x}(0) = 1, \quad \tilde{\phi}(0) = 1. \tag{47}$$

Here we have assumed for simplicity that  $n > 1$  and introduced a dimensionless constant,

$$\lambda_{rd} \stackrel{\text{def}}{=} \lim_{\lambda \rightarrow \infty} \left( \frac{\lambda}{x_0^\nu} \right). \tag{48}$$

The definition of  $\delta_{rd}$  is given in Eq. (42).

The four boundary conditions (47) allow us to integrate the two first-order equations (46) and to determine the two ‘‘eigenvalues’’  $\delta_{rd}$  and  $\lambda_{rd}$ . The asymptotical behavior,

$$x_0|_{\lambda \rightarrow \infty} = \left( \frac{\lambda}{\lambda_{rd}} \right)^{1/\nu}, \quad \sigma_0|_{\lambda \rightarrow \infty} = \delta_{rd} \left( \frac{\lambda_{rd}}{\lambda} \right)^{1/\nu}, \tag{49}$$

implied by Eqs. (42) and (48), is actually established by the fact that the eigenvalue problem (46), (47) has a unique solution with  $0 < \lambda_{rd}, \delta_{rd} < \infty$  (and  $\delta_{rd} < 1$ ). The latter can be proven analytically and is easy to verify numerically for  $n > \nu$  and  $n > 1$ . By integrating Eqs. (46) further into the  $v > 0$  domain, we calculate  $v_{rd+}$  and  $\tilde{\sigma}_{rd+}$  defined in Eq. (44). Table III lists the values of  $\lambda_{rd}$ ,  $\delta_{rd}$ ,  $v_{rd+}$ , and  $\tilde{\sigma}_{rd+}$  for a selection of  $n, \nu$  pairs.

Equations (45)–(47) describe a particular case of our self-similar solution which corresponds to the asymptotical regime of strongly non-adiabatic implosions. We call it a radiatively dominated regime because the energy is assumed to be lost by radiation. For the particular set (19) of the matter and geometry parameters this solution is plotted in Fig. 4. It corresponds to the critical value of the parameter  $c_a = 0.409871$  in Ref. 13. When  $n = \nu + 1$ , Eqs. (46) admit an analytical solution given in Appendix B.

A radiatively dominated (RD) regime sets in whenever the initial conditions stipulate that the timescale for the entropy loss (as evaluated along the adiabatic trajectory) is much shorter than the hydrodynamic timescale. Then, the imploding mass loses most of its initial entropy before coming to a halt. As a result, the information about the initial entropy is essentially ‘‘forgotten,’’ and the implosion pro-

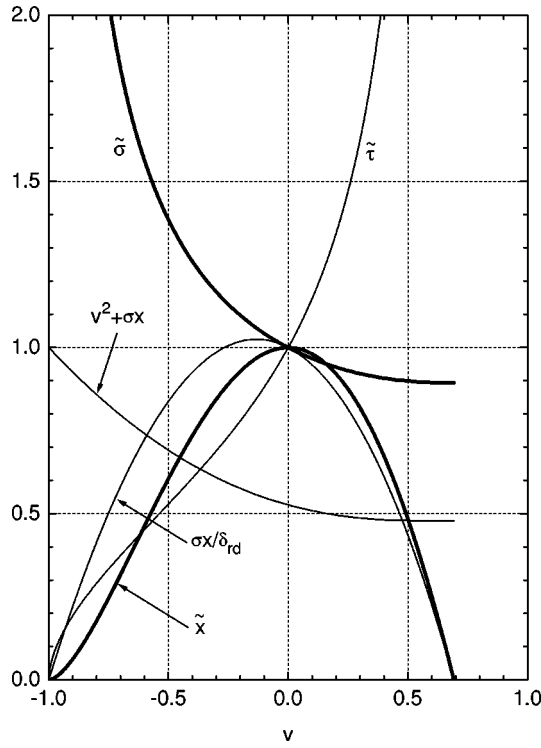


FIG. 4. Integral curves for the system (46) of the radiatively dominated regime calculated with the basic set (19) of geometry and material parameters.

ceeds as if having started from the infinite initial entropy. This is illustrated by the  $\tilde{\sigma}$  curve in Fig. 4. Note that, although the peak of the central temperature (the  $\sigma x/\delta_{rd}$  curve) occurs before (at  $v = -0.13$ ) the very moment of stagnation, the kinetic energy by that time is already negligibly small.

As might be expected, the stagnation parameters in the RD regime do not depend on the initial entropy  $\Sigma_-$  and are fully determined by the mass and initial velocity (or, equivalently, initial energy) of the imploding configuration. Substituting asymptotical expressions (49) into Eqs. (36), (37), and (40), we calculate the central temperature  $T_{rd}$ , density  $\rho_{rd}$ , and confinement parameter  $\langle \rho r \rangle_{rd}$  at stagnation in the RD regime,

$$T_{rd} = \delta_{rd} T_{a0} = \delta_{rd} a U_-^2, \tag{50}$$

$$\rho_{rd} = \left( \frac{\beta \kappa_* (\gamma - 1) a^{n-1} U_-^{2n-1}}{\lambda_{rd} M_*^{1/(s+1)}} \right)^{(s+1)/(ms+m+s)}, \tag{51}$$

$$\langle \rho r \rangle_{rd} = I_\rho \left( \frac{\beta \kappa_* (\gamma - 1) a^{n-1} U_-^{2n-1} M_*^{m/s}}{\lambda_{rd}} \right)^{s/(ms+m+s)}. \tag{52}$$

**D. Adequacy of the heat conduction approximation**

Applicability of the heat conduction approximation to describe radiative energy losses requires that the Rosseland optical thickness,

$$\tau = \int_0^{R\xi_1} l_R^{-1} dr = \tau_{a0} \cdot \sigma^{3-n} x^{3-n+\mu} \geq 1. \tag{53}$$

Here

$$\tau_{a0} = \frac{I_\tau}{l_*} \frac{M_*^{1/(s+1)}}{(a U_-^2)^{n-3-\mu} \Sigma_-^\mu}, \quad I_\tau = \int_0^{\xi_1} \frac{\Pi^m d\xi}{Z^{m+n-3}}, \tag{54}$$

$$\mu = \frac{m(s+1) - 1}{(\gamma - 1)(s+1)} = \nu - \frac{1}{\gamma - 1}. \tag{55}$$

In a quasi-adiabatic implosion,  $\tau = \tau(v)$  is minimum at stagnation—as is illustrated with the  $\tau/\tau_{a0}$  curve for  $\lambda = 0$  in Fig. 3—provided that  $n > 3 + \mu$  (for  $\gamma = 5/3$  the latter inequality,  $n > \nu + 3/2$ , is more restrictive than the condition  $n > \nu$  assumed throughout this section). Hence, it is sufficient to verify that  $\tau(0) \equiv \tau_{a0} \geq 1$ .

For strongly non-adiabatic implosions the situation is more complicated because, as the value of  $\lambda$  increases, the minimum of  $\tau(v)$  shifts to negative  $v$ , i.e., to earlier times before the stagnation (see Fig. 3). In the asymptotical limit of the RD regime,

$$\tau(v) = \tau_{rd} \cdot \tilde{\tau}(v) = \tau_{rd} \cdot \tilde{\sigma}^{3-n} \tilde{x}^{3-n+\mu} \tag{56}$$

is a monotonically increasing function of  $v$  (see Fig. 4). Hence, the condition

$$\tau(0) \equiv \tau_{rd} = \frac{I_\tau \delta_{rd}^{3-n}}{l_*} \left[ \left( \frac{\beta \kappa_* (\gamma - 1)}{\lambda_{rd}} \right)^{ms+m-1} \times \frac{a^{(2m-n)(s+1)+3s+1} M_*^{1/(ms+m+s)}}{U_-^{(2n-5m)(s+1)-6s-1}} \right] \geq 1 \tag{57}$$

is weaker than inequality (53) and does not guarantee the applicability of the RD solution to the entire process of implosion for very large  $\lambda$ . If, for example, we would like to apply it to the  $\lambda = 100$  case in Fig. 3, we would have to require  $\tau(0) > 5$  in order to have  $\tau(v) > 1$  over the entire range  $-1 < v < v_+$ . Hence, inequality (57) should be considered as only a necessary condition for applicability of the RD solution, and, unless  $\tau_{rd} \gg 1$ , the conclusions obtained should be checked with a more adequate model for radiative cooling.

**E. Application to ICF**

A conventional approach to ICF relies on a spherical implosion of 0.1–10 mg of DT fuel to achieve high compression needed for thermonuclear ignition.<sup>7</sup> We can apply the present self-similar solution to investigate the effect of radiative cooling on the implosion dynamics of fuel configurations which have no hot spot in the center and, therefore, would be appropriate for the volume ignition and the compression stage of the fast ignitor schemes of ICF.

Following the conventional parametrization of ICF implosions, we introduce the implosion velocity  $U_{im}$  defined by

$$E_- = \frac{1}{2} M U_{im}^2, \tag{58}$$

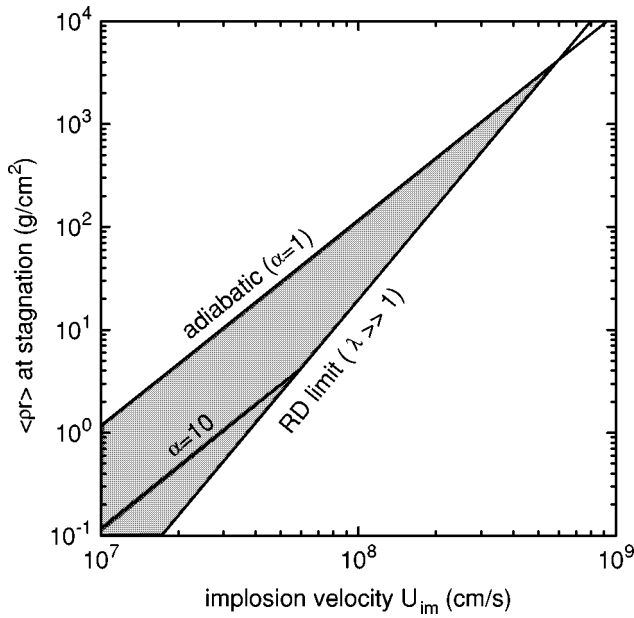


FIG. 5. Accessible values (shaded region) of the  $\langle \rho r \rangle$  parameter at stagnation versus implosion velocity for 1 mg of DT.

where  $E_-$  is the initial total energy of the imploding fuel of mass  $M$ . The fuel entropy is characterized by the dimensionless compressibility parameter,

$$\alpha \stackrel{\text{def}}{=} \frac{P}{P_{deg}} = 10^{-13} \bar{A}^{5/3} \Sigma, \quad (59)$$

where  $p_{deg} = 10^{13} (\rho/\bar{A})^{5/3}$  is the Fermi pressure of degenerate electrons, and  $p$ ,  $\rho$ , and  $\Sigma$  are in the CGS units. Below we use the  $\alpha$  value corresponding to the center of the imploding mass. All practical formulae in this subsection are given for a fully ionized arbitrary mixture of hydrogen isotopes with the mean atomic mass  $\bar{A}$  (for the equimolar DT mixture  $\bar{A} = 2.5$ ). We adopt the basic set (19) of the geometry and matter parameters and use the following expression for the Rosseland mean free path due to the inverse bremsstrahlung,<sup>2</sup>

$$l_R [\text{cm}] = 70.68 g^{-1} \bar{A}^{-2} \rho^{-2} T_{keV}^{7/2}. \quad (60)$$

Here  $T_{keV}$  is the temperature in keV, and  $g$  is the appropriately averaged value of the Gaunt factor. For the hydrogen plasma at  $T \approx 3$  keV one calculates  $g \approx 0.4$  in the Elwert approximation.<sup>21</sup> To keep track of the opacity scaling, we retain the factor  $g$  explicitly in the formulae below.

First of all, we apply our solution with a goal to establish a boundary in the parameter space which separates the adiabatic and non-adiabatic regimes in the final stage of the fuel implosion. To this end, we plot two limiting lines on the  $\log U_{im}$ ,  $\log \langle \rho r \rangle$  plane as shown in Fig. 5. The first line, obtained from Eq. (38) and given by the relationship

$$\langle \rho r \rangle_{\alpha 0} [\text{g/cm}^2] = 0.255 \bar{A}^{5/3} \alpha^{-1} M_{mg}^{1/3} U_{im,7}^2, \quad (61)$$

with  $\alpha = 1$ , corresponds to the maximum possible  $\langle \rho r \rangle$  values that can be achieved at stagnation by imploding the fuel adiabatically along the zero isentrope; here  $M_{mg}$  is the fuel

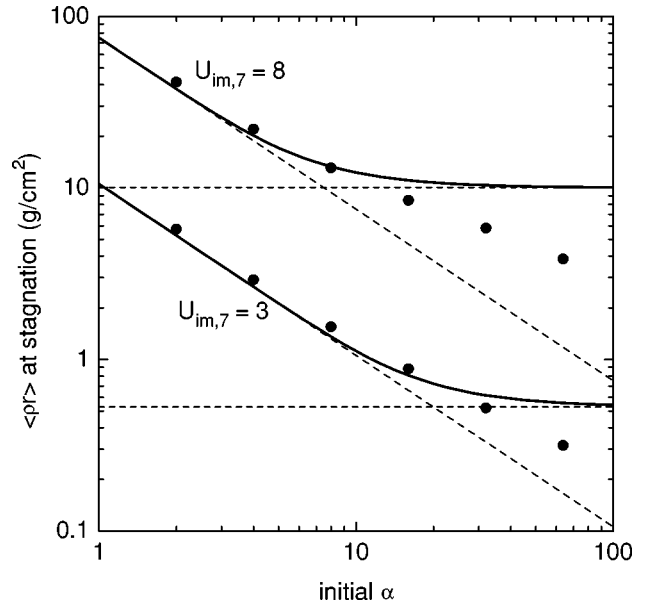


FIG. 6. Confinement parameter at stagnation versus initial value of the entropy parameter  $\alpha$  for two values of the implosion velocity for 1 mg of DT. Predictions of the self-similar solution (solid curves) are compared with the one-dimensional hydrodynamic simulations (black dots). The adiabatic and the RD limits are shown as the oblique and horizontal dashed lines.

mass in mg, and  $U_{im,7}$  is the implosion velocity in  $10^7$  cm/s. Note that, although the self-similar solution does not account for the effects of electron degeneracy in the equation of state, the limit of adiabatic implosion of a partially (or fully) degenerate configuration is still rigorously recovered from it (provided that the  $\alpha$  values are restricted to  $\alpha \geq 1$ ) because the non-relativistic Boltzmann and Fermi electrons both have the same adiabatic index of  $\gamma = 5/3$ .

The second limiting line in Fig. 5, given by the equation

$$\langle \rho r \rangle_{rd} [\text{g/cm}^2] = 1.77 \times 10^{-3} g^{-1/4} \bar{A}^{-19/8} M_{mg}^{1/4} U_{im,7}^3, \quad (62)$$

and plotted for  $g = 0.4$ ,  $\bar{A} = 2.5$ ,  $M_{mg} = 1$ , corresponds to the RD regime. The self-similar solution predicts that only the  $\langle \rho r \rangle$  values in the shaded region between the two curves (61) and (62) can be realized at stagnation. Note that in reality, when the effects of electron degeneracy are properly accounted for, the RD limiting curve should approach the  $\alpha = 1$  line only asymptotically.

If, now, we draw an adiabatic line (61) for any other value of  $\alpha > 1$  (as it is illustrated with the  $\alpha = 10$  curve in Fig. 5), it will cross the RD line at a point beyond which the adiabatic approximation breaks down. Hence, we obtain the following criterion:

$$\alpha U_{im,7} < 144 g^{1/4} \bar{A}^{-17/24} M_{mg}^{1/12} = 60 M_{mg}^{1/12} |_{\text{DT}}, \quad (63)$$

for the adiabatic behavior of the final stage of the fuel implosion. The factor  $g^{1/4}$  in Eq. (63) defines the opacity scaling, which manifests how the domain of adiabatic implosions would expand when the DT fuel is doped (or contaminated) with other elements.

Transition from the adiabatic to a strongly non-adiabatic regime of implosion is illustrated in Fig. 6. Here we consider

how the final fuel  $\langle \rho r \rangle$  at stagnation,  $\langle \rho r \rangle_0$ , changes as we increase the initial fuel entropy characterized by the value  $\alpha_-$  of the parameter  $\alpha$  (as defined by the value of  $\Sigma_-$ ), keeping the DT fuel mass and its implosion velocity fixed. In the adiabatic approximation, the  $\langle \rho r \rangle_0$  values fall along the slanting dashed lines inversely proportional to  $\alpha_-$ , as indicated by Eq. (61). The transition to the non-adiabatic regime, as predicted by the self-similar solution, is shown with the solid curves: for large enough values of  $\alpha_-$ , the  $\langle \rho r \rangle$  at stagnation ceases to depend on  $\alpha_-$  and approaches asymptotically the RD limit indicated with the horizontal dashed lines. Because, however, the condition on the Rosseland optical thickness along the RD line,

$$\tau_{rd} = 0.716 g^{3/8} \bar{A}^{-7/16} M^{1/8} U_{im,7}^{1/2} > 1, \tag{64}$$

is only marginally (and only at  $U_{im} \gtrsim 2 \times 10^7$  cm/s) satisfied for  $M \approx 1$  mg, we have performed in addition one-dimensional three-temperature hydrodynamics simulations with the DEIRA code<sup>18</sup> to verify the predictions of the self-similar solution. The results are shown in Fig. 6 with black dots. In these simulations the effects of Fermi degeneracy have been properly accounted for. The initial state was assigned at the radius  $R = 4R_{a0}$  in accordance with the isentropic self-similar profiles for  $\alpha$  being constant over the fuel mass.

The results presented in Fig. 6 demonstrate that the criterion (63) delimits quite accurately the domain in the parameter space where the final stage of the fuel implosion can still be treated adiabatically. However, because the imploding DT masses of interest to ICF are only marginally optically thick and partially degenerate, the RD regime predicted by the self-similar solution is never actually reached, although the tendency to approach it over a certain range of parameters (especially for high values of  $U_{im}$ ) is quite conspicuous.

Similarly, one can evaluate the reduction of the central fuel temperature  $T_c(0)$  at stagnation in the non-adiabatic regime as compared to the adiabatic one: according to the self-similar solution, this reduction is limited by the factor  $\delta_{rd}^{-1}$ , with the values of  $\delta_{rd}$  listed in Table III.

Thus, by applying our self-similar solution to the final stage of the fuel implosion in the context of volume ignition and cold precompression for fast ignition, we obtain quantitative information [criterion (63)] on where in the parameter space radiative energy losses become important, and qualitative information on how the fuel parameters at stagnation are altered by these losses.

### V. EXPLOSION TYPE SOLUTIONS

The RD solution of Sec. IV C, which starts formally with the infinite initial entropy, describes the asymptotical implosion flow in the limit when it becomes independent of the initial entropy because most of this entropy has been radiated away. A similar solution exists for the asymptotical regime of radiative explosion, when a gaseous mass initially at rest is very rapidly heated to such a high initial temperature that most of the initial entropy is radiated away before the gas begins to move. This solution is governed by the

same equations (11)–(13) but with different initial conditions for  $R(t)$  and  $T_c(t)$ . The initial state is now fully specified by the values of two parameters  $R_0 = R(0)$  and  $\rho_0 = \rho_c(0)$  (or, equivalently, by  $R_0$  and  $M_* = \rho_0 R_0^{s+1}$ ). The initial temperature, entropy, and thermal energy are infinite, while the initial velocity  $\dot{R}(0) = 0$ .

Having normalized  $R(t)$  to  $R_0$ , we can use one degree of freedom available for normalization of  $\dot{R}(t)$  and  $\Sigma(t)$  to reduce the temporal components of Eqs. (12) and (13) to the simplest form,

$$\frac{dx}{dv} = -2v \phi^{1/(n-1)}, \tag{65a}$$

$$\frac{d\phi}{dv} = x^{n-\nu-1}, \tag{65b}$$

where

$$x = \left( \frac{R_0}{R(t)} \right)^{(\gamma-1)(s+1)}, \quad v = \frac{\dot{R}(t)}{U_0}, \quad \phi = \sigma^{1-n}, \tag{66}$$

$$\sigma = \frac{\Sigma(t)}{\Sigma_0}, \quad \Sigma_0 = a U_0^2 \rho_0^{1-\gamma}, \tag{67}$$

$$U_0 = \left( \frac{\rho_0^{m+1} R_0}{\beta \kappa_* (\gamma-1)(n-1) a^{n-1}} \right)^{1/(2n-1)}. \tag{68}$$

Equations (65) must be integrated from  $v=0$  to  $v=v_{ex+}$  with the boundary conditions

$$x(0) = 1, \quad \phi(0) = 0, \quad x(v_{ex+}) = 0. \tag{69}$$

The corresponding integral curves for the basic set (19) are plotted in Fig. 7 together with the Rosseland optical thickness,

$$\tau(v) = \tau_0 \cdot \sigma^{3-n} x^{3-n+\mu}, \quad \tau_0 = \frac{I_\tau}{l_*} \frac{\rho_0^m R_0}{(a U_0^2)^{n-3}}. \tag{70}$$

Note that Eqs. (46) of the RD implosion regime can also be renormalized to (65) but with different initial conditions.

Having calculated the values of  $v_{ex+}$  and  $\sigma_{ex+} \equiv \sigma(v_{ex+})$  by integrating Eqs. (65), we find the asymptotical (in the limit of  $t \rightarrow +\infty$ ) values of the entropy parameter,

$$\Sigma_+ \stackrel{\text{def}}{=} \Sigma(+\infty) = \Sigma_0 \cdot \sigma_{ex+}, \tag{71}$$

and the total (equal to the kinetic) energy,

$$E_+ \stackrel{\text{def}}{=} E(+\infty) = \frac{1}{2} (4\pi)_s (s+1) I_{\Pi} M_* U_0^2 \cdot v_{ex+}^2, \tag{72}$$

of the expanding gas.  $E_+$  is the residual energy left over in the gas after it cools down to the non-radiating stage. Numerical values of  $v_{ex+}$  and  $\sigma_{ex+}$  for a selection of  $n, \nu$  pairs are listed in Table III. Analytical expressions for the case of  $n = \nu + 1$  are given in Appendix B.

The asymptotical regime of radiative expansion considered here occurs when a macroparticle with initial density  $\rho_0$  and size  $R_0$  is very rapidly (on a timescale of  $t \lesssim t_r$ ) volumetrically heated to such a high temperature  $T$  that the timescale of radiative cooling,  $t_r = \rho_0 R_0^2 / \kappa$ , becomes shorter than

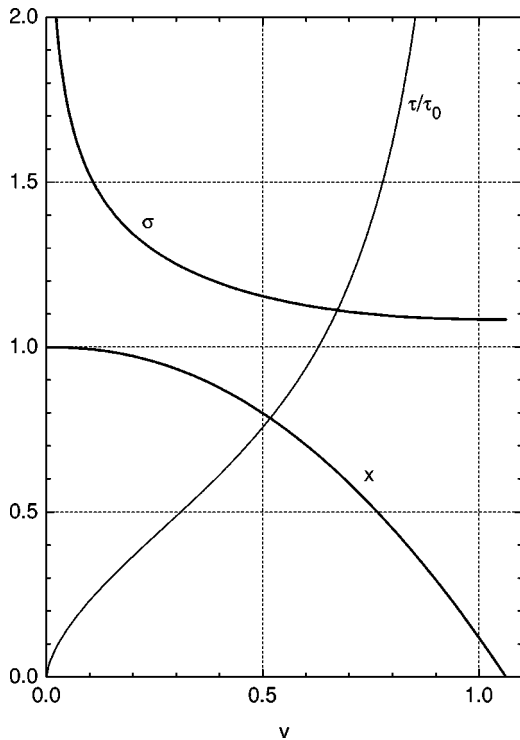


FIG. 7. Integral curves for the system (65) of the explosion solution calculated with the basic parameter set (19). Shown also is the normalized Rosseland optical thickness  $\tau/\tau_0$ .

the hydrodynamic timescale  $t_h = R_0 T^{-1/2}$ . When combined with the constraint  $\tau \gtrsim 1$  on the Rosseland optical thickness, the latter condition can be expressed as

$$1 \lesssim \frac{R_0}{l_R(\rho_0, T)} \ll \frac{16}{3} \frac{T^{5/2}}{\sigma_{SB} \rho_0}. \tag{73}$$

This condition is, for example, satisfied for 30–50  $\mu\text{m}$  particles of solid gold heated to a temperature of  $T \approx 2$  keV on a timescale of  $t \lesssim 10$  ps, or for  $\approx 2$  mm particles of solid aluminum heated to  $T \approx 1$  keV on a timescale of  $t \lesssim 1$  ns. Volumetric heating of such intensity is encountered when high power laser and particle beams interact with matter.

**VI. SUMMARY**

We have demonstrated that the equations of one-dimensional hydrodynamics with heat conduction admit a self-similar solution which can be used to investigate the effects of radiative cooling on the implosion dynamics of thermonuclear fuel in ICF targets. With the aid of this solution we find that the radiative energy losses can—at least in principle — enhance the density and the  $\langle \rho r \rangle$  parameter at maximum compression by an arbitrarily large factor. At the same time, no more than a finite fraction on the order of 50% of the initial energy can be lost in this way. In the limit of intense radiative cooling the flow pattern approaches an asymptotical RD regime, in which the flow parameters near stagnation become independent of the initial entropy and are fully determined by the mass and initial energy of the imploding mass.

The conclusions formulated above are based on two main assumptions, namely that (i) the equation of state is that of the ideal gas, and (ii) the Rosseland optical thickness of the imploding configuration is greater than unity. Because these conditions are only marginally fulfilled for implosions of DT masses in the milligram range relevant to ICF, the RD regime is never really reached in such implosions and not all the predictions of the self-similar solution have a sufficient quantitative accuracy. Nevertheless, the solution proves to be quite helpful in clarifying the qualitative effects of radiative cooling on the dynamics of ICF implosions and yields a fairly accurate criterion (63) for the domain where these effects can still be ignored.

Besides the implosion type of flows, there exists a branch of our self-similar solution which describes the asymptotical regime of hydrodynamic expansion after a certain mass is very rapidly heated to such a temperature that the timescale of radiative cooling becomes shorter than the hydrodynamic timescale. In such a case the self-similar solution enables one to calculate the residual kinetic energy of the expanding plasma.

**ACKNOWLEDGMENTS**

We want to acknowledge stimulating discussions with K. Mima.

This work was supported in part by INTAS under the contract No. 93-2571.

**APPENDIX A: MATHEMATICAL PROPERTIES OF THE EIGENVALUE PROBLEM**

For  $\beta > 0$  Eq. (14b) implies  $dZ/d\xi \leq 0$ , which means that  $Z(\xi) < 1$  and, by virtue of Eq. (14a), that

$$\Pi(\xi) \leq \exp(-\xi^2/2). \tag{A1}$$

In the limit of  $\beta \ll 1$  we can assume  $0 \leq 1 - Z \ll 1$  and obtain the following approximate solution to Eqs. (14):

$$\Pi(\xi) \approx e^{-\xi^2/2}, \tag{A2a}$$

$$Z^{n+m+1}(\xi) \approx 1 - \beta(n+m+1)$$

$$\times \int_0^\xi \frac{dy}{y^s} e^{-my^2/2} \int_0^y \zeta^s e^{-\zeta^2/2} d\zeta, \tag{A2b}$$

which extends to  $\xi_1 = \infty$ . As it follows from Eq. (A1), the integral on the rhs of Eq. (A2b) converges for any  $m > 0$ , which justifies the assumption  $1 - Z \ll 1$  above.

In the opposite limit of  $\beta \gg 1$ , an approximate solution to Eq. (14b) can be obtained by assuming  $0 \leq 1 - \Pi \ll 1$ ,

$$Z^{n+m+1}(\xi) \approx 1 - \frac{\beta(n+m+1)}{2(s+1)} \xi^2. \tag{A3}$$

This solution extends to  $\xi_1 = [\beta(n+m+1)/2(s+1)]^{-1/2} \ll 1$ , and by integrating Eq. (14a) with  $Z$  from Eq. (A3) we verify that  $1 - \Pi(\xi_1) \ll 1$  for any  $n, m > 0$ . Thus, for  $\beta \ll 1$  we have  $0 = \Pi(\xi_1) < Z(\xi_1) \approx 1$ , while for  $\beta \gg 1$  we have  $0 = Z(\xi_1) < \Pi(\xi_1) \approx 1$ . Clearly, there must exist an intermediate value of  $\beta$  for which  $\Pi(\xi_1) = Z(\xi_1) = 0$ .

Having assumed that the value of  $\xi_1$  is finite, Eq. (14b) can be integrated from  $\xi=0$  to  $\xi \rightarrow \xi_1$  to yield

$$Z|_{\xi \rightarrow \xi_1} = \frac{m\xi_1}{m+n} (\xi_1 - \xi), \quad (\text{A4a})$$

$$\Pi|_{\xi \rightarrow \xi_1} = C \left( \frac{m\xi_1}{m+n} \right)^{1+(n+1)/m} (\xi_1 - \xi)^{1+n/m}, \quad (\text{A4b})$$

where

$$C = \left( \beta \xi_1^{-s} \int_0^{\xi_1} \xi^s \Pi d\xi \right)^{-1/m}. \quad (\text{A5})$$

Note that the density profile,  $\Pi(\xi)/Z(\xi)$ , also vanishes at  $\xi = \xi_1$  as  $(\xi_1 - \xi)^{n/m}$ . It can be shown that an infinite value of  $\xi_1$  would be incompatible with the requirements  $\lim_{\xi \rightarrow \infty} \Pi(\xi) = \lim_{\xi \rightarrow \infty} Z(\xi) = 0$  for  $m, n > 0$ .

The asymptotical formulae (A4) together with the conditions  $d\Pi(0)/d\xi = dZ(0)/d\xi = 0$  suggest the following simple approximations for  $\Pi(\xi)$  and  $Z(\xi)$ :

$$Z \approx 1 - \left( \frac{\xi}{\xi_1} \right)^2, \quad \Pi \approx Z^{1+n/m}. \quad (\text{A6})$$

By comparing the above expression for  $Z$  with Eq. (A4a), we infer an approximate formula for  $\xi_1$ ,

$$\xi_1 \approx \left[ 2 \left( 1 + \frac{n}{m} \right) \right]^{1/2}. \quad (\text{A7})$$

## APPENDIX B: ANALYTICAL RESULTS FOR A SPECIAL CASE OF $n = \nu + 1$

In the particular case of  $n = \nu + 1$ , Eqs. (33) can be easily integrated to yield

$$\sigma = [1 + \lambda \nu (1 + \nu)]^{-1/\nu}, \quad (\text{B1a})$$

$$x = 2 \frac{1 + \lambda \nu}{\nu(\nu + 1)\lambda^2} \{ [1 + \lambda \nu (1 + \nu)]^{1+1/\nu} - 1 \} - \frac{1}{\nu(\nu + 1/2)\lambda^2} \{ [1 + \lambda \nu (1 + \nu)]^{2+1/\nu} - 1 \}. \quad (\text{B1b})$$

From this solution we calculate the values of the principal parameters, defined in Eqs. (48), (42), and (44), which characterize the radiatively dominated regime,

$$\lambda_{rd} = \frac{1}{\nu} \left[ \frac{(\nu + 1/2)(\nu + 1)}{\nu^2} \right]^\nu, \quad (\text{B2})$$

$$\delta_{rd} = \frac{\nu^2}{(\nu + 1/2)(\nu + 1)}, \quad (\text{B3})$$

$$\nu_{rd+} = \frac{\nu}{\nu + 1}, \quad \tilde{\sigma}_{rd+} = \left( \frac{\nu + 1}{2\nu + 1} \right)^{1/\nu}. \quad (\text{B4})$$

Also, Eqs. (46) of the RD regime can be directly integrated to yield

$$\tilde{\sigma} = (1 + \nu)^{-1/\nu}, \quad (\text{B5a})$$

$$\tilde{x} = (1 + \nu)^{1+1/\nu} \left( 1 - \frac{\nu + 1}{\nu} \nu \right). \quad (\text{B5b})$$

For the explosion solution of Sec. V we obtain

$$\sigma = \nu^{-1/\nu}, \quad x = 1 - \frac{\nu}{\nu + 1/2} \nu^{2+1/\nu}, \quad (\text{B6})$$

$$\nu_{ex+} = \left( 1 + \frac{1}{2\nu} \right)^{\nu/(2\nu+1)}, \quad \sigma_{ex+} = \left( 1 + \frac{1}{2\nu} \right)^{-1/(2\nu+1)}. \quad (\text{B7})$$

<sup>1</sup>L. I. Sedov, *Similarity and Dimensional Methods in Mechanics* (Academic, New York, 1959).

<sup>2</sup>Ya. B. Zel'dovich and Yu. P. Raizer, *Physics of Shock Waves and High Temperature Hydrodynamic Phenomena* (Academic, New York, 1966).

<sup>3</sup>S. V. Coggeshall and R. A. Axford, *Phys. Fluids* **29**, 2398 (1986).

<sup>4</sup>R. Pakula and R. Sigel, *Phys. Fluids* **28**, 232 (1985).

<sup>5</sup>R. Sigel, R. Pakula, S. Sakabe, and G. D. Tsakiris, *Phys. Rev. A* **38**, 5779 (1988).

<sup>6</sup>M. Murakami and J. Meyer-ter-Vehn, *Nucl. Fusion* **31**, 1315 (1991); **31**, 1333 (1991).

<sup>7</sup>J. Lindl, *Phys. Plasmas* **2**, 3933 (1995).

<sup>8</sup>M. Basko, *Phys. Plasmas* **3**, 4148 (1996).

<sup>9</sup>P. Reinicke and J. Meyer-ter-Vehn, *Phys. Fluids A* **3**, 1807 (1991).

<sup>10</sup>V. V. Neudachin and P. V. Sasorov, *Nucl. Fusion* **33**, 475 (1993).

<sup>11</sup>R. Kishony, E. Waxman, and D. Shvarts, *Phys. Plasmas* **4**, 1385 (1997).

<sup>12</sup>M. Murakami, M. Shimoide, and K. Nishihara, *Phys. Plasmas* **2**, 3466 (1995).

<sup>13</sup>M. Murakami, *Nucl. Fusion* **37**, 549 (1997).

<sup>14</sup>R. E. Kidder, *Nucl. Fusion* **16**, 3 (1976).

<sup>15</sup>M. Schwarzschild, *Structure and Evolution of Stars* (Princeton University Press, Princeton, 1958).

<sup>16</sup>H. Hora, *Plasmas at High Temperature and Density* (Springer-Verlag, Berlin, 1991).

<sup>17</sup>J. D. Lindl, in *Inertial Confinement Fusion*, Proceedings of the Course and Workshop, Varenna, 1988 (Editrice Compositori, Bologna, 1989), pp. 595 and 617.

<sup>18</sup>M. M. Basko, *Nucl. Fusion* **30**, 2443 (1990).

<sup>19</sup>S. Atzeni, *Jpn. J. Appl. Phys., Part 1* **34**, 1980 (1995).

<sup>20</sup>M. Tabak, J. Hammer, M. E. Glinsky, W. L. Kruer, S. C. Wilks, J. Woodworth, E. M. Campbell, and M. D. Perry, *Phys. Plasmas* **1**, 1626 (1994).

<sup>21</sup>G. Elwert, *Ann. Phys.* **34**, 178 (1939).